Comparative analysis of metabolic and transcriptomic features of Nothobranchius furzeri

Maria Rita Fumagalli,[1,2] Francesc Font-Clos,[3] Simone Milan,[2] Stefano Zapperi,[3,4] and Caterina A. M. La Porta[2,1,5]

[1] *CNR - Consiglio Nazionale delle Ricerche, Biophysics institute, via De Marini 6, Genova, Italy*

[2] *Center for Complexity and Biosystems, Department of Environmental Science and Policy, University of Milan, via Celoria 26, 20133 Milano, Italy*

[3] *Center for Complexity and Biosystems, Department of Physics, University of Milan, via Celoria 16, 20133 Milano, Italy*

[4] *CNR - Consiglio Nazionale delle Ricerche, Istituto di Chimica della Materia Condensata e di Tecnologie per l'Energia, Via R. Cozzi 53, 20125 Milano, Italy*

[5] *Innovation for Well-Being and Environment (CR-I-WE), University of Milan, Milan, Italy.*

Abstract

Some species have a longer lifespan than others, but usually the lifespan is correlated with the typical body weight. Here, we study the lifetime evolution of the metabolic behavior of Nothobranchius furzeri (*N. furzeri*), a killifish with an extremely short lifespan with respect to other fishes, even when considering a proper rescaling by body weight. Comparison of the gene expression patterns of *N. furzeri* with those of zebrafish *D. rerio* and mouse (*M. musculus*), shows that a broad set of metabolic genes and pathways are deregulated in *N. furzeri* during aging in a way that is consistent with a global opening of the chromatin. Computational analysis of the glycolysis pathway for the three species highlights a much rapid increase in the metabolic activity during lifetime for *N. furzeri* with respect to the other species. Our results highlight that the unusually short lifespan of *N. furzeri* is associated to peculiar patterns in the metabolic activities and in chromatin dynamics.

INTRODUCTION

Nothobranchius furzeri (*N. furzeri*) is a species of killifish from the family Nothobranchiidae which live in pools in semi-arid areas with scarce and erratic precipitations in Africa. Due to its very short captive lifespan ranging from 3 to 12 months depending on the environment [7], it is considered by the scientific community as an attractive live model for aging [15]. In a recent paper, a longitudinal study in *N. furzeri* showed quantitative correlation between gene expression variations during early adult life and lifespan [5]. Under the same conditions, it was also demonstrated that the mitochondrial respiratory chain complex I is a hub in a module of genes whose expression is negatively correlated with lifespan [5]. An interesting result was obtained treating both *N. furzeri* and *D. rerio* with rotenone, an inhibitor of complex I, demonstrating a rejuvenating effect on the transcriptome [5].

Other studies in the literature reported on the mechanism of aging in *N. furzeri* in comparison to mammals, showing some similar traits including shortening of telomeres, mitochondrial disfunctions, aging-associated upregulation of translation and ribosomal processes and reduced regenerative capacity [24]. Herein, our aim was to understand in more depth the aging behavior of *N. furzeri* in comparison with other fishes, using as model *D. rerio* who has a longer lifespan. To achieve this result, we compared transcriptomes, gene distances and metabolic genes and pathways of *N. furzeri* with respect to *D. rerio* in three different tissues (brain, liver and skin) at five different time points, ranging from sexual maturity up to average lifetime. We also compared under the same conditions our results with *M. musculus*, as a mammalian example, to show if different mechanisms are displayed during aging in different vertebrates (fishes versus mammals).

MATERIALS AND METHODS

Lifespan analysis

Lifespan and weight of all available species were downloaded from the Fishbase online database [9]. For those species whose weight was not available, we estimated it weight using the formula $a * L^b$ [6] where the length L and the parameters a, b were obtained from Fishbase. When more than one value was available for a single species, we considered the average value. As a whole, we were able to obtain data on 1002 species. Additionally, we

considered the parameter K of dimension $year^{-1}$ that essentially describes the growth speed of a species, being related to the exponential growth of its size [9]. Maximal longevity and weight of 332 teleosts were obtained from AnAge database [28]. Additionally, for five short-lived species lacking data in AnAge, we obtained the average weight from the literature: Crystallogobius linearis 0.2035g [18], Cyclothone braueri 0.25g[2], Electrona risso 2.7g[4], Eucyclogobius newberryi 0.83g [27], Galaxiella nigrostriata 0.09 g [11].

Lifetime and weight of eight different species of Nothobranchius (*N.furzeri* MZM and GRZ,*N.kilomberoensis*, *N.rachovii*, *N.korthausae*,*N.kuhntae* MT 03/04 and Beira, and *N. guentheri*) were obtained from literature when missing from AnAge and Fishbase datasets [12, 16, 19, 21, 29–32, 34]. while Eviota sigillata and *N.furzeri* weight were set to 0.09g and 3g respectively according to Fishbase model. Duplicated data between the two datasets were removed, preferring AnAge data.

Transcriptomic data and gene annotation

We considered data of *N. furzeri* (strain MZM-04/10), *D. rerio* and *M. musculus* transcriptomes from three different tissues (brain, liver and skin) at five different time points, ranging from sexual maturity up to average lifetime. In particular, *N. furzeri* data refer to animals 5, 12, 20, 27, 39 weeks old, while *D. rerio* and *M. musculus* samples were sequenced at 6, 12, 24, 36, 42 and 2, 9, 15, 24, 30 months of age respectively. Note that the last two time points refer to highly different probability of survival in each species (Fig. S1). In particular last time point corresponds to survival rate $\approx$50% for *D. rerio* and *M. musculus* while only $\approx$25% of *N. furzeri* individuals survive up to 39 weeks. For each species at each time point five replica were available. All RNA-Seq data were published before and are accessible at NCBIs Gene Expression Omnibus (*N. furzeri*: GSE52462 and GSE66712, *D. rerio*: GSE74244, *M. musculus*: GSE75192)[1, 3]. *N. furzeri* raw sequences were aligned to reference transcriptome ($Nfu_20140520$ [25]) using StringTie (v.1.3 [23]). For each transcriptome, genes with more than 10 counts in at least one time point were considered as expressed in a given tissue. This subset of genes was used as background reference for enrichment analysis. Genes annotated as belonging to HDACs and HATs class and specific polycomb genes were selected for all the species using NCBI [22] annotation file, and additional hand-curated annotation from Uniprot was performed for *D. rerio* and *M.*

musculus.

Differentially expressed genes

Differential expression analysis was performed using EdgeR ([26], R package version 3.12.1), considering only genes with more than 10 raw counts in at least one time point implementing default Benjamini-Hochberg correction. For each time point, $\log_2$ expression of the fold change ($log2FC$) compared to the first time point was calculated and genes with corrected $p-value < 0.05$ were considered as differentially expressed. Reactions containing at least one DE gene were considered as deregulated.

Gene distance distribution

The distribution of genomic distances between expressed genes for each tissue in each species has been obtained calculating the distance occurring between the end of a gene and the beginning of the next one. Random sampling (10^3 replica) was performed on the distributions in order to compare random inter-gene distances with the clustering occurring between either up or down-regulated genes. The sample size was chosen to be equal to the number of differentially expressed genes at each time point. Kolmogorov-Smirnov test was used to compare random distribution with DE genes distribution using python [33].

Metabolic genes and pathways

Metabolic pathways, reactions and related genes were downloaded from Kegg ([17], last accession September 2018). A total of 1691 reactions belonging to 76 pathways and grouped in 11 superpathways involving genes expressed in at least one time point were considered. Reactions containing at least one DE gene were considered as deregulated. For *D. rerio* and *M. musculus*, KeggLinkDB [10] and BioMart [14] were used to map Kegg genes on RNA-seq data.

Model for metabolic deregulation

We use a constrain-based model where each reaction flux is a variable v_i and each internal species imposes a mass constrain, as its overall production/consumption must balance to zero. Some species are allowed to be out of balance, however, as they are inputs/outputs of the pathway. Considering only internal species, the mass-balance condition can be expressed as $A \cdot \vec{v} = 0$ where A is the stoichiometric matrix of the pathway. We also take into account reaction reversibilities, imposing that $v_i > 0$ for irreversible reactions, and add a minimal flux constrain $|v_i| > v_{\min}$ for all reactions to avoid numerical issues during fold-change calculations, see next section. Putting these three sets of constraints together, and denoting the set of irreversible reaction indices by $\mathcal{I}$, we define the set of feasible fluxes $\mathcal{V}$ as

$$\mathcal{V} = \{\vec{v} \in \mathbb{R}^N : A \cdot \vec{v} = 0;\ v_i > 0\, \forall i \in \mathcal{I};\ |\vec{v}_i| > v_{\min} \forall i\}$$

As the number of chemical reactions is larger than the number of internal species, the system is underdetermined and there are many possible solutions to the problem, represented by the set $\mathcal{V}$. Notice that we do not impose any further growth-related objective function –as is typical in flux-balance analysis approaches. Instead, we propose a fold-change based fitting mechanism for which no objective function is needed.

Model fitting

We assume that enzymatic abundances are proportional to reaction fluxes. That is,

$$v_i(x_i) = \alpha_i x_i \tag{1}$$

where x_i is the experimental enzymatic abundance associated to reacion i, v_i is the correspondent model reaction flux and α_i an unkown, reaction-dependent proportionality constant. It is clear that without access to the value of α_i we cannot compare absolute values of x_i and v_i. However, we can work at the level of fold changes without needing to determine the proportionality constants, as

$$\frac{v_i(\lambda x_i)}{v_i(x_i)} = \frac{\alpha_i \lambda x_i}{a_i x_i} = \lambda \tag{2}$$

In other words, we can associate a foldchange of factor λ in the model to a foldchange of the same factor in the experimental enzymatic abundancies. Repeating this argument for all reactions, we find the pair of fluxes $(\vec{u}, \vec{v})$ that better approximate the experimental fold-changes. To do so, we define the squared total logarithmic error of a pair of model fluxes $\vec{u}, \vec{v}$ given a pair of experimental values $\vec{x}, \vec{y}$ as follows:

$$F(\vec{u}, \vec{v}|\vec{x}, \vec{y}) = \sum_{i=1}^{N} \left[\log\left(\frac{\vec{u}_i}{\vec{v}_i}\right) - \log\left(\frac{\vec{x}_i}{\vec{y}_i}\right) \right]^2$$

The best fit of the model to the data $\vec{x}, \vec{y}$ is defined as the pair of feasible fluxes $\vec{u}, \vec{v} \in \mathcal{V}$ that minimize $F(\vec{u}, \vec{v}|\vec{x}, \vec{y})$, and are found numerically using the minimize function from scipy.optimize python library.

Efficiency estimation

We define the efficiency of the glycolisis pathway as

$$\eta = \frac{|p|}{|g|}$$

with p, g the pyruvate and glucose fluxes. The change in efficiency $\Delta\eta$ betweem two timepoints can be defined as $\Delta\eta = \frac{\eta_1}{\eta_0}$. Is is easy to see that this quantity can be computed from the changes of glucose and pyruvate.

$$\Delta\eta = \frac{\eta_1}{\eta_0} = \frac{|p_1|/|g_1|}{|p_0|/|g_0|} = \frac{\Delta p}{\Delta g}$$

In turn, we can estimate $\Delta p, \Delta g$ from the pair of solutions that better approximates the experimental data fold changes, see above for details.

In summary, it is possible to estimate how the glycolysis pathway efficiency change during time by fitting a constrain-based model to enzymatic abundancies data.

RESULTS

Allometric scaling of *N. furzeri* in comparison with other fish

To better appreciate the exceptionally short life span of *N. furzeri*, we compared its properties to other fish species. Since a meaningful comparison could only be performed

by taking into account also the relative body mass or body length of different species, we collected data on the total lifespan and weight for different fish species as detailed in the materials and methods section. Furthermore, we considered the growth speed of each fish species, encoded by the parameter K.

In Fig. 1a, we report a logarithmic plot of the lifetimes of 1441 fish species and 10 Nothobranchius species as a function of their weight. Regression analysis shows a relation between lifetimes LT and weight W scaling as $(LT) \propto (W)^{0.2}$. Nothobranchius species are reported in red. A plot of the lifetimes rescaled by their weight as $LT/W^{0.20}$. Fig. 1b shows that Nothobranchius species are in the left tail of the distribution, meaning that they live less than what would be expected for fishes of the same weight. Nothobranchius furzeri GRZ is the most extreme outlier since its value differs from the mean by more than four standard deviations (4σ), while Nothobranchius furzeri MZM differs by 2σ.

Similar results were obtained considering the growth rate K which we report in Fig. 1c for 2109 fish species and 3 Nothobranchius species as a function of their weight. Here, the fit yielded a power law with exponent -0.15. Again, when growth rates (K) were rescaled by weights (W) as $K/W^{-0.15}$, both Nothobranchius Nothobranchius furzeri GRZ and MZM are roughly 4σ above the mean (Fig. 1d).

Global deregulation of gene expression in *N. furzeri*, *D. rerio* and *M. musculus*

We evaluated differentially expressed (DE) genes from transcriptomes obtained from three different tissues (brain, liver and skin) of short-lived turquoise killifish *N. furzeri* as well as *D. rerio* and *M. musculus* in the same conditions (see Materials and Method section). As comparison, we also analyzed *M. musculus* under the same conditions. Figure 2a shows that, while *D. rerio* and *M. musculus* have a similar percentage of DE genes, *N. Furzeri* shows a larger fraction of DE genes during aging. Moreover, when we compared single tissues or each time point and for a specific functional categories we obtained the same trend (Fig. S2).

We then investigated if a particular pattern of deregulation occurred, comparing the distribution of DE genes on the genome with an appropriate null-model distribution where we assess its degree of randomness. In other words, our aim was to understand if the deregulated genes are randomly sampled throughout the genome or if they are localized

into particular regions across the genome. Our analysis shows that the distribution of DE genes is dramatically different between the species and tissues (Fig.2b). In fact, *D. rerio* shows a general non-random distribution of DE genes, while, *N. furzeri* DE genes appears to be randomly distributed along the genome in all the considered cases. *M. musculus*, in contrast, shows a completely different pattern with respect to both fishes, displaying a tissue and time specific regulation with an increasing clustering of upregulated DE genes during ageing (Fig.2b).

Since these data seems to suggest that the process of ageing in *N. furzeri* is related to a global, uniform deregulation of chromatin state, we investigated the changes in expression of genes involved in chromatin remodeling such as polycomb repressor complex 1 and 2 (PRC1 and PRC2) (BM1, RING, Ezh2 and Suz12), histone deacetylase (HDAC) and histone acetyltransferase (HAT) genes. As shown in 3, we found a specific and strong signal of deregulation in *N. furzeri* with a marked and constant decrease of PCR2 genes (Ezh2 and Suz12) and a slight increase of PCR1 (BM1 and RING) genes in late time points (see Fig. 3). Considering HDAC and HAT genes. Figure 3 *N. furzeri* shows a complex picture of DE genes in skin, liver and brain, completely different with respect to *D. rerio* where none of the genes is significantly deregulated (Fig. 4. *M. musculus* also shows a different pattern in comparison to fishes and in particular brain does not show any DE HDAC or HAT genes (Fig. 4). The expression of most deregulated HAT and HDAC genes including Kat2a, Kat2b, Hdac4, Hdac8 and Hdac9 show a coherent expression through the different tissues and the opposite trend of genes belonging to different classes of deacetylase complexes can be attributed to their different role (see Fig. S3), coherently with observations reported in humans [13].

Modeling changes in metabolic pathways of *N. furzeri*, *D. rerio* and *M. musculus* during ageing process

To investigate the possible origin of the shorter lifespan of *N. furzeri* with respect to *D. rerio*, we focused on possible differences in their metabolic activity. As a further comparison, *M. musculus* during aging was also considered. Metabolic networks for the three species were derived from the Kegg database [17]. In the three species, the global structure of the network is conserved, showing a good agreement in terms of compounds and reactions (see Fig. S4).

In order to highlight possible deregulation of metabolic network, DE genes annotated as enzyme were mapped on the metabolic network and reactions catalyzed by at least one DE gene were considered as deregulated (for more details see Materials and Method section). Figure 5 shows that, for all the three organisms, the skin tissue has the highest amount of deregulated reactions for each category of metabolic pathway. When the three species are compared *N. furzeri* shows an higher number of deregulated superpathways, that is even more evident when we observe data at single-pathway level (Fig. S5).

In order to verify if deregulated reactions defined in terms of DE genes led to changes in terms of efficiency in the production and consumption of metabolites, we implemented a model based on flux balance analysis. We applied our model to curateD version of the fundamental glycolysis pathway, that is an ideal candidate to define metabolic efficiency. The model, described in details the Material and Methods section, allows to measure changes in glycolysis efficiency (defined as the ratio between glucose income and pyruvate production) as a function of time based on gene expression changes. Figure 6 reports the relative change of efficiency at each time point in comparison to the initial one. Detectable changes in glycolysis were observed in liver and skin tissue, while in all the three organisms brain efficiency is essentially constant (Figure 6). Noticeably, *N. furzeri* shows an increased of pyruvate production, in accordance with an increase of metabolic rate during ageing, while *D. rerio* efficiency decrease.

DISCUSSION

Every organism ages, but understanding the basic mechanisms of aging is a longstanding open problem in evolutionary biology. Here we investigated this aspect considering *N. furzeri*, a species of killifish from the family Nothobranchiidae which has a significantly shorter lifespan with respect to other fishes, including *D. rerio* [7], even when the age is properly rescaled by the fish weight. We addressed two main questions: 1) are differences in aging behavior due to a specific core of genes or it is a more global process involving a complex gene deregulation? 2) Are aging mechanisms distinct in different vertebrates?

To address the first question, our strategy was to compare the transcriptomes of *N. furzeri* in three different tissues (brain, liver and skin) at five different time points, ranging from sexual maturity up to average lifetime, with respect to *D. rerio* and quantify the percentage

of deregulated genes. We found that *N. furzeri* has a larger fraction of genes deregulated (45%) with respect to *D. rerio*. We found a similar percentage of deregulated genes in *D. rerio* and in *M. musculus*. We then computed the distribution of genomic distances between expressed genes in each species, comparing it with a null distribution obtained picking random genes from each genome. Thus, we could measure, using a KS test, how likely DE genes are randomly distributed along the genome. We used the Kolmogorov-Smirnov test to compare the DE genes cluster distribution with a random cluster distribution. We found that in *N. furzeri* the DE genes cluster distribution did not significantly deviate from the one obtained in a random cluster null model. On the other hand, in *D. rerio* and more clearly in *M. musculus* we found a clear non-random deregulation pattern, confirming that *N. furzeri* shows a global gene deregulation.

In order to investigate in more depth the impact of aging on the biology of these vertebrates, we focused our attention on genes involved in chromatin remodeling such as polycombs genes. Polycomb functions are performed by multiprotein complexes that selectively occupy chromatin sites. They are usually subdivided into two main classes: Polycomb repressive complex 1 and 2 (PRC1 and PRC2) [20]. Polycomb genes of both classes are almost constantly expressed in *M. musculus* while there is a larger varibility in their expression in *D. rerio*, where the different pattern of expression of bmi1a and bmi1b could indicate a slightly different role of these protein during zebrafish lifetime [8]. Our analysis shows instead a clear deregulation of polycomb genes in *N. furzeri* suggesting that chromatin is accessiblile in all the analyzed tissues and at all the time points. *D. rerio* and more clearly *M. musculus* show a less open chromatin and a smaller percentage of deregulated genes.

Since chromatin remodeling is due to the dynamic modification of chromatin architecture allowing for access of condensed genomic DNA to the regulatory transcription machinery proteins, and thereby controlling gene expression, we also investigated deregulation of histone acetyltransferases (HATs) and histone deacetylase (HDAC) genes. We found a deregulation of these genes in *N. furzeri* with respect to *M.Musculus* and *D. rerio* in all three different tissues (brain, liver and skin) at all time points. All together these results show a global deregulation and open chromatin in the short-lived *N. furzeri* without any specific pattern of organization of these genes. In *D. rerio* we found less deregulation and a more organized patterns of deregulated genes. In *M. musculus*, the situation is similar but even more clearly organized into patterns and there is a very low deregulation of the genes.

To investigate whether we can observe an impact of gene deregulation at an higher level of complexity, we analyzed metabolic pathways and reactions deregulation, using a a reference Kegg database [17] for a total of 1691 reactions belonging to 76 pathways. We also grouped the genes in 11 super pathways when the genes was expressed in at least one time point and the reactions contained at least one DE gene were considered as deregulated. While the structure of the metabolic pathways was the same for all the three species considered, we found a high deregulation of the reaction in *N. furzeri* considering the super pathways. To confirm this results, we introduced a network-based model to analyze the glicolysis efficiency defined as the ratio of glucose to pyruvate transformation, a conserved pathway, showing changes in liver and skin tissue among the species, while in all the three organisms brain efficiency is essentially constant. Noticeably, *N. furzeri* shows an increase of pyruvate production as the metabolic rate increases during ageing, while in *D. rerio* the efficiency decreases in time.

Altogether, our results show that the short lifespan of *N. furzeri*, even when properly rescaled by its body weight, is due to a peculiar metabolic and chromatin dynamics that is very different not only from other fish species but also from mammals. It is only thanks to a comparative analysis of the time dependence of the metabolic and gene expression activity in fishes that one can fully appreciate the peculiarity of the aging behavior of *N. furzeri*. This can be seen an example of exaptation in which the same gene and pathways common to all fishes are used in a different way by *N. furzeri*. On the hand, the aging behavior in mammals is closer to the one observed in fish like *D. rerio* rather than the one in *N. furzeri*.

[1] P. Aramillo Irizar, S. Schäuble, D. Esser, M. Groth, C. Frahm, S. Priebe, M. Baumgart, N. Hartmann, S. Marthandan, U. Menzel, J. Müller, S. Schmidt, V. Ast, A. Caliebe, R. König, M. Krawczak, M. Ristow, S. Schuster, A. Cellerino, S. Diekmann, C. Englert, P. Hemmerich, J. Sühnel, R. Guthke, O.W. Witte, M. Platzer, E. Ruppin, and C. Kaleta. Transcriptomic alterations during ageing reflect the shift from cancer to degenerative diseases in the elderly. *Nature Communications*, 9(1), 2018.

[2] Julian Badcock and Nigel Robert Merrett. Midwater fishes in the eastern north atlantic—i. vertical distribution and associated biology in 30 n, 23 w, with developmental notes on certain

myctophids. *Progress in Oceanography*, 7(1):3–58, 1976.

[3] T. Barrett, D.B. Troup, S.E. Wilhite, P. Ledoux, C. Evangelista, and I.F. Kim. Ncbi geo: archive for functional genomics data sets - 10years on. *Nucleic Acids Res*, 39, 01 2012.

[4] Pietro Battaglia, Franco Andaloro, Valentina Esposito, Antonia Granata, Letterio Guglielmo, Rosanna Guglielmo, Simona Musolino, Teresa Romeo, and Giacomo Zagami. Diet and trophic ecology of the lanternfish electrona risso (cocco 1829) in the strait of messina (central mediterranean sea) and potential resource utilization from the deep scattering layer (dsl). *Journal of Marine Systems*, 159:100–108, 2016.

[5] Mario Baumgart, Steffen Priebe, Marco Groth, Nils Hartmann, Uwe Menzel, Luca Pandolfini, Philipp Koch, Marius Felder, Michael Ristow, Christoph Englert, Reinhard Guthke, Matthias Platzer, and Alessandro Cellerino. Longitudinal rna-seq analysis of vertebrate aging identifies mitochondrial complex i as a small-molecule-sensitive modifier of lifespan. *Cell Syst*, 2(2):122–32, 02 2016.

[6] E. Cinco. *Length-weight relationships of fishes.* ICLARM Tech. Rep. 7, 1982.

[7] Amber Dance. Live fast, die young. *Nature*, 535(7612):453–5, 07 2016.

[8] B. Dupret, P. Völkel, X.L. Bourhis, and P.-O. Angrand. The polycomb group protein pcgf1 is dispensable in zebrafish but involved in early growth and aging. *PLoS ONE*, 11(7), 2016.

[9] R Froese and D Pauly. *FishBase 2000: concepts, design and data sources. ICLARM, Los Ban os.* ICLARM, Laguna, Philippines., 2000.

[10] W. Fujibuchi, S. Goto, H. Migimatsu, I. Uchiyama, A. Ogiwara, Y. Akiyama, and M. Kanehisa. Dbget/linkdb: an integrated database retrieval system. *Pacific Symposium on Biocomputing. Pacific Symposium on Biocomputing*, pages 683–694, 1998.

[11] David M Galeotti. Metapopulation theory explains black-stripe minnow (pisces: Galaxiidae, galaxiella nigrostriata) distribution in seasonal wetlands in south-west western australia. 2013.

[12] Tyrone Genade, Mauro Benedetti, Eva Terzibasi Tozzini, Paola Roncaglia, Dario Valenzano, Antonino Cattaneo, and Alessandro Cellerino. Annual fishes of the genus nothobranchius as a model system for aging research. *Aging cell*, 4:223–33, 11 2005.

[13] C.M. Grozinger and S.L. Schreiber. Regulation of histone deacetylase 4 and 5 and transcriptional activity by 14-3-3-dependent cellular localization. *Proceedings of the National Academy of Sciences of the United States of America*, 97(14):7835–7840, 2000.

[14] Jonathan M. Guberman, J. Ai, O. Arnaiz, Joachim Baran, Andrew Blake, Richard Baldock,

Claude Chelala, David Croft, Anthony Cros, Rosalind J. Cutts, A. Di Génova, Simon Forbes, T. Fujisawa, E. Gadaleta, D. M. Goodstein, Gunes Gundem, Bernard Haggarty, Syed Haider, Matthew Hall, Todd Harris, Robin Haw, S. Hu, Simon Hubbard, Jack Hsu, Vivek Iyer, Philip Jones, Toshiaki Katayama, R. Kinsella, Lei Kong, Daniel Lawson, Yong Liang, Nuria Lopez-Bigas, J. Luo, Michael Lush, Jeremy Mason, Francois Moreews, Nelson Ndegwa, Darren Oakley, Christian Perez-Llamas, Michael Primig, Elena Rivkin, S. Rosanoff, Rebecca Shepherd, Reinhard Simon, B. Skarnes, Damian Smedley, Linda Sperling, William Spooner, Peter Stevenson, Kevin Stone, J. Teague, Jun Wang, Jianxin Wang, Brett Whitty, D. T. Wong, Marie Wong-Erasmus, L. Yao, Ken Youens-Clark, Christina Yung, Junjun Zhang, and Arek Kasprzyk. BioMart Central Portal: an open database network for the biological community. *Database*, 2011, 09 2011. bar041.

[15] Itamar Harel, Bérénice A Benayoun, Ben Machado, Param Priya Singh, Chi-Kuo Hu, Matthew F Pech, Dario Riccardo Valenzano, Elisa Zhang, Sabrina C Sharp, Steven E Artandi, and Anne Brunet. A platform for rapid exploration of aging and diseases in a naturally short-lived vertebrate. *Cell*, 160(5):1013–1026, Feb 2015.

[16] Michael Herrera and Pudur Jagadeeswaran. Annual fish as a genetic model for aging. *The journals of gerontology. Series A, Biological sciences and medical sciences*, 59:101–7, 03 2004.

[17] Minoru Kanehisa, Miho Furumichi, Mao Tanabe, Yoko Sato, and Kanae Morishima. KEGG: New perspectives on genomes, pathways, diseases and drugs. *Nucleic acids research*, 45, 11 2016.

[18] Mario La Mesa. Age and growth of crystallogobius linearis (von düben, 1845)(teleostei: Gobiidae) from the adriatic sea. *Scientia Marina*, 65(4):375–381, 2001.

[19] Alejandro Lucas Sánchez, Pedro Almaida-Pagán, J.A. Madrid, Jorge de Costa Ruiz, and Pilar Mendiola. Age-related changes in fatty acid profile and locomotor activity rhythms in nothobranchius korthausae. *Experimental gerontology*, 46:970–8, 08 2011.

[20] Raphaë l Margueron and Danny Reinberg. The polycomb complex prc2 and its mark in life. *Nature*, 469(7330):343–9, Jan 2011.

[21] A. Markofsky, J.and Perlmutter. Age at sexual maturity and its relationship to longevity in the male annual cyprinodont fish, nothobranchius guenther. *Experimental Gerontology*, 7:131–135, 04 1972.

[22] Nuala A O'Leary, Mathew W Wright, J Rodney Brister, Stacy Ciufo, Diana Haddad, Rich

McVeigh, Bhanu Rajput, Barbara Robbertse, Brian Smith-White, Danso Ako-Adjei, et al. Reference sequence (refseq) database at ncbi: current status, taxonomic expansion, and functional annotation. *Nucleic acids research*, 44(D1):D733–D745, 2016.

[23] Mihaela Pertea, Daehwan Kim, Geo M Pertea, Jeffrey T Leek, and Steven L Salzberg. Transcript-level expression analysis of rna-seq experiments with hisat, stringtie and ballgown. *Nature protocols*, 11(9):1650, 2016.

[24] Matthias Platzer and Christoph Englert. Nothobranchius furzeri: A model for aging research and more. *Trends Genet*, 32(9):543–552, 09 2016.

[25] Kathrin Reichwald, Andreas Petzold, Philipp Koch, Bryan R Downie, Nils Hartmann, Stefan Pietsch, Mario Baumgart, Domitille Chalopin, Marius Felder, Martin Bens, et al. Insights into sex chromosome evolution and aging from the genome of a short-lived fish. *Cell*, 163(6):1527–1538, 2015.

[26] M.D. Robinson, D.J. McCarthy, and G.K. Smyth. edger: a bioconductor package for differential expression analysis of digital gene expression data. *Bioinformatics*, 26:139–140, 2010.

[27] Ramona O Swenson. The ecology, behavior, and conservation of the tidewater goby, eucyclogobius newberryi. *Environmental Biology of Fishes*, 55(1-2):99–114, 1999.

[28] Robi Tacutu, Daniel Thornton, Emily Johnson, Arie Budovsky, Diogo Barardo, Thomas Craig, Eugene Diana, Gilad Lehmann, Dmitri Toren, Jingwei Wang, et al. Human ageing genomic resources: new and updated databases. *Nucleic acids research*, 46(D1):D1083–D1090, 2018.

[29] Eva Terzibasi Tozzini, Alexander Dorn, Enoch Ng'oma, Matej PolaIk, Radim Blaek, Kathrin Reichwald, Andreas Petzold, Brian Watters, Martin Reichard, and Alessandro Cellerino. Parallel evolution of senescence in annual fishes in response to extrinsic mortality. *BMC evolutionary biology*, 13:77, 04 2013.

[30] Eva Terzibasi Tozzini, Christel Lefrancois, Paolo Domenici, Nils Hartmann, Michael Graf, and Alessandro Cellerino. Effects of dietary restriction on mortality and age-related phenotypes in the short-lived fish nothobranchius furzeri. *Aging cell*, 8:88–99, 05 2009.

[31] Eva Terzibasi Tozzini, Dario Valenzano, Mauro Benedetti, Paola Roncaglia, Antonino Cattaneo, Luciano Domenici, and Alessandro Cellerino. Large differences in aging phenotype between strains of the short-lived annual fish nothobranchius furzeri. *PloS one*, 3:e3866, 02 2008.

[32] Stefano Valdesalici and Alessandro Cellerino. Extremely short lifespan in the annual fish

nothobranchius furzeri. *Proceedings. Biological sciences / The Royal Society*, 270 Suppl 2:S189–91, 12 2003.

[33] Pauli Virtanen, Ralf Gommers, Travis E. Oliphant, Matt Haberland, Tyler Reddy, David Cournapeau, Evgeni Burovski, Pearu Peterson, Warren Weckesser, Jonathan Bright, Stéfan J. van der Walt, Matthew Brett, Joshua Wilson, K. Jarrod Millman, Nikolay Mayorov, Andrew R. J. Nelson, Eric Jones, Robert Kern, Eric Larson, CJ Carey, İlhan Polat, Yu Feng, Eric W. Moore, Jake Vand erPlas, Denis Laxalde, Josef Perktold, Robert Cimrman, Ian Henriksen, E. A. Quintero, Charles R Harris, Anne M. Archibald, Antônio H. Ribeiro, Fabian Pedregosa, Paul van Mulbregt, and SciPy 1. 0 Contributors. SciPy 1.0: Fundamental Algorithms for Scientific Computing in Python. *Nature Methods*, 2020.

[34] Sebastian Wendler, Nils Hartmann, Beate Hoppe, and Christoph Englert. Agedependent decline in fin regenerative capacity in the shortlived fish nothobranchius furzeri. *Aging cell*, 14, 06 2015.

FIGURES

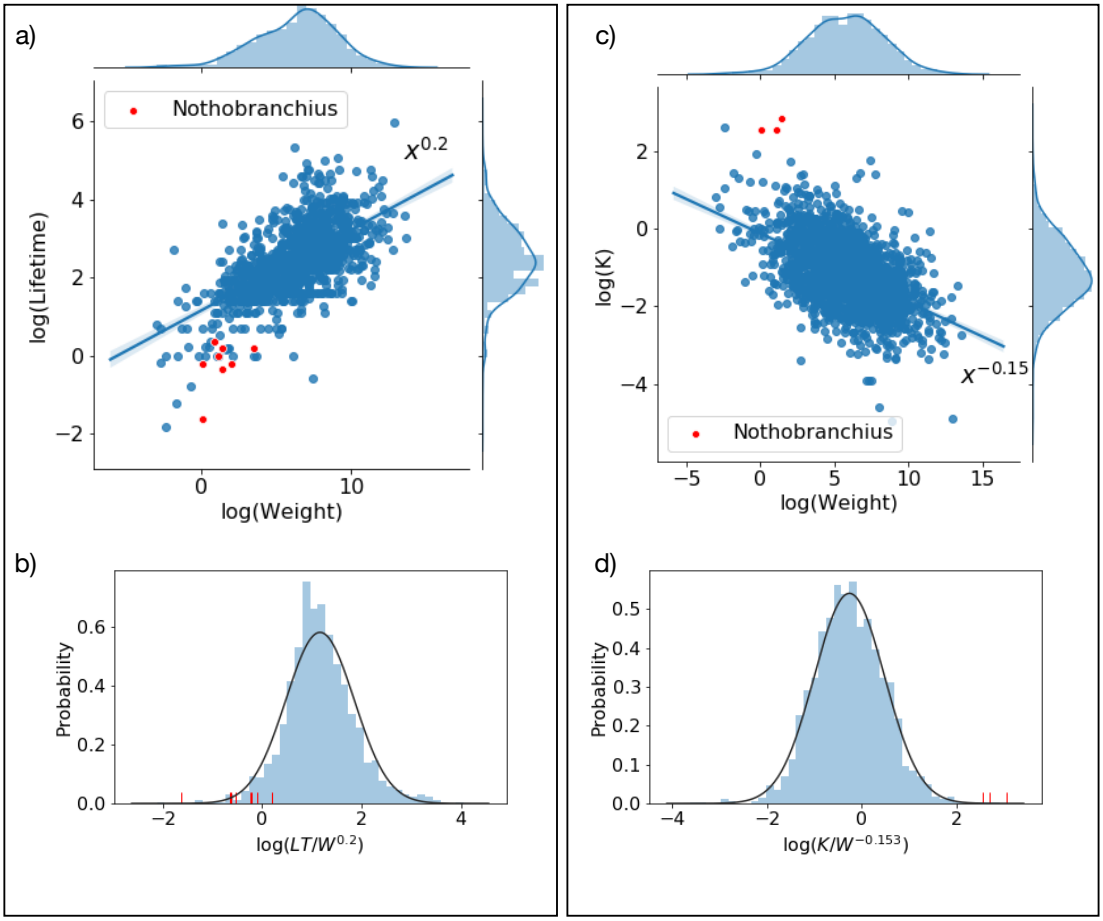

FIG. 1. **Allometric scaling of fish**. a) The lifetimes of 1441 fish species and 10 Nothobranchius species are plotted against their weight in a log-log plot. The fit yields a power law with exponent 0.20. b) When lifetimes (LT) are rescaled by weights (W) as $LT/W^{0.20}$, Nothobranchius species all appear in the left-hand side of the distribution, particularly Nothobranchius furzeri GRZ. c) The growth rate K of 2109 fish species and 3 Nothobranchius species are plotted against their weight in a log-log plot. The fit yields a power law with exponent -0.15. d) When growth rates (K) are rescaled by weights (W) as $K/W^{-0.15}$, Nothobranchius species all appear in the right-hand side of the distribution, particularly Nothobranchius furzeri GRZ.

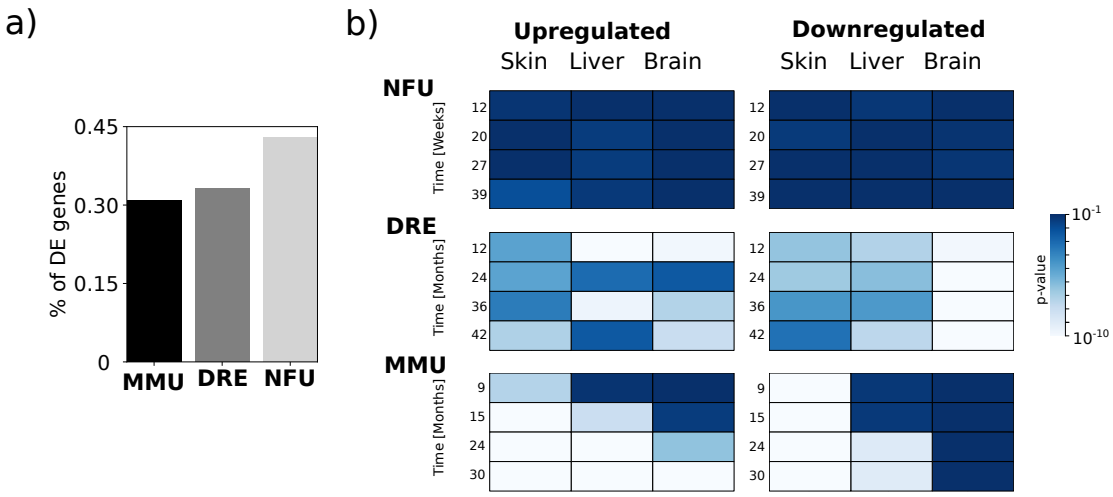

FIG. 2. **Deregulated genes during ageing process**. a) Fraction of genes differentially expressed in the three species (MMU=*M. musculus*; DRE=*D. rerio*; NFU=*N. furzeri*) in at least one time point. b)Probability that, at each time, genes differentially expressed are randomly distributed along the genome. The distribution of genomic distances between differentially regulated genes has been compared with the distribution obtained from random sampling of expressed genes for each species. Heatmap reports the average p-value obtained comparing inter-gene distances distribution using KS test (10^3 replica) Higher p-values indicate a distribution close to the null-model random distribution.

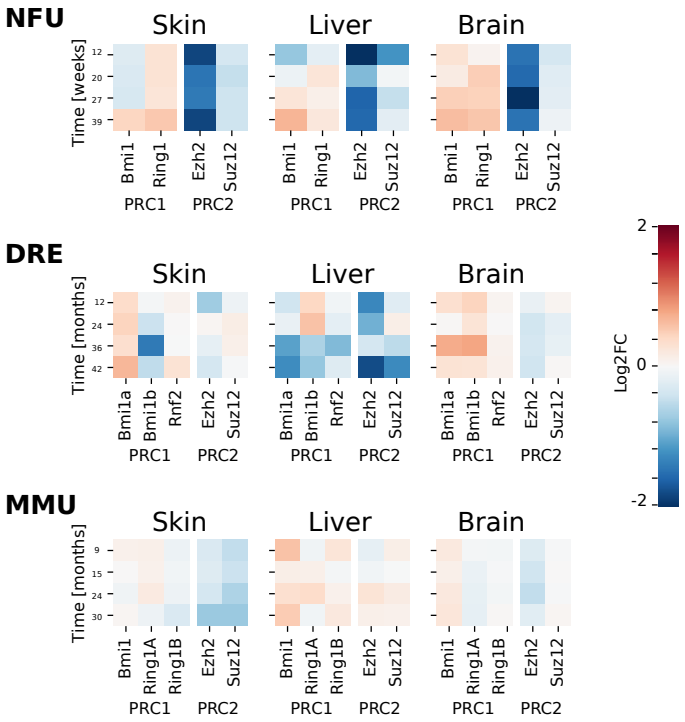

FIG. 3. **Expression of polycomb repressive complex 1 and 2**. Figure shows changes of expression of a set of genes belonging to polycomb repressive complex 1 (PCR1) and polycomb repressive complex 2 (PCR2) classes in the different species as a function of time. Expression is reported as log2FC compared to initial time point.

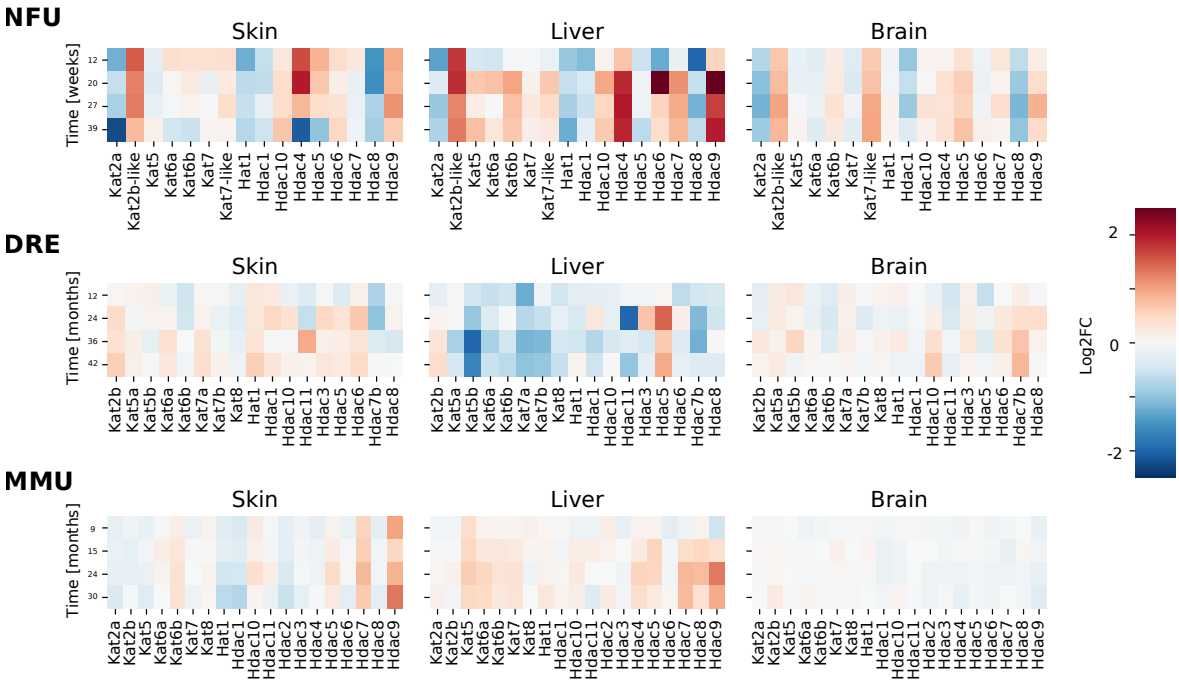

FIG. 4. **Differentially expressed HDACs and HATs genes**. Figure shows the log2FC expression relative to initial time point of genes belonging to HDACs or HATs (Kat) classes. Expression is reported as log2FC compared to initial time point. MMU=*M. musculus*; DRE=*D. rerio*; NFU=*N. furzeri*.

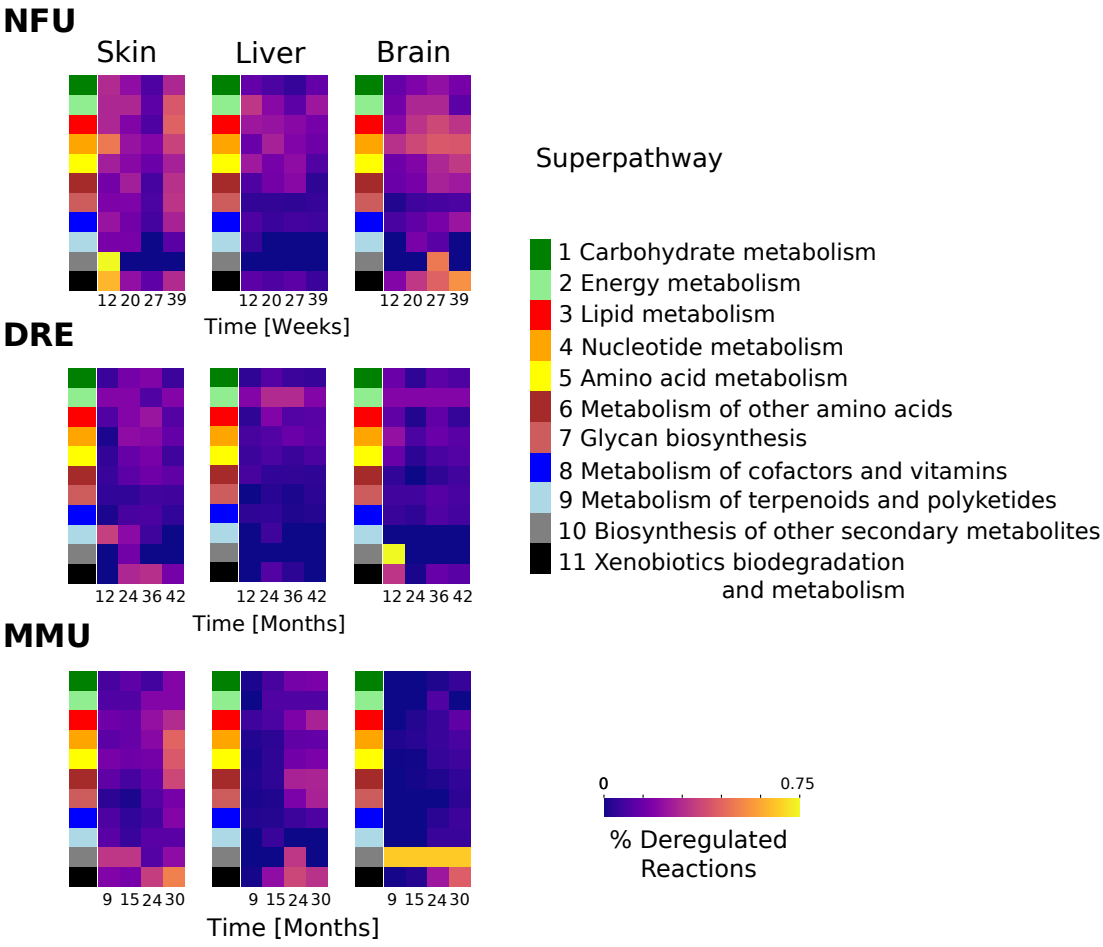

FIG. 5. **Deregulated metabolic reactions**. Metabolic reactions containing at least one differentially expressed gene are considered as deregulated. Heatmaps show the percentage of deregulated metabolic reactions for each superpathway (see legend) as a function of time. MMU=*M. musculus*; DRE=*D. rerio*; NFU=*N. furzeri*.

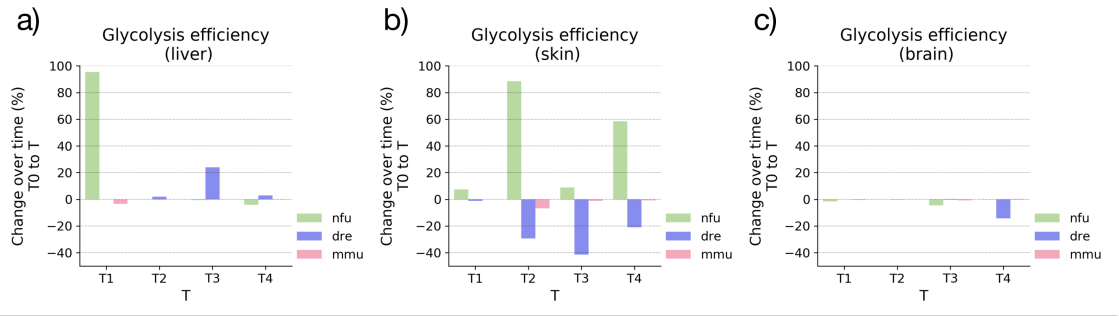

FIG. 6. **Change in glycolysis efficiency over time** Barplots displaying the change in glycolysis efficiency, defined as the ratio of glucose to pyruvate transformation, as estimated by the constraint-based metabolic model. The bars show the relative change in efficiency at a given timepoint T with respect to the initial time T_0 for *N.Furzeri* (green), zebrafish (blue), mouse (pink) and three different tissues: liver (a), skin (b) and brain (c). Overall, the figure shows how NFU increases its efficiency during its lifetime. MMU=*M. musculus*; DRE=*D. rerio*; NFU=*N. furzeri*.